Mechanical behavior of ultrafine-grained Al composites reinforced with B$_4$C nanoparticles

Zhihui Zhang,[a,*] Troy Topping,[a] Ying Li,[a] Rustin Vogt,[a] Yizhang Zhou,[a] Chris Haines,[b] Joseph Paras,[b] Deepak Kapoor,[b] Julie M. Schoenung[a] and Enrique J. Lavernia[a]

[a]Department of Chemical Engineering and Materials Science, University of California, Davis, CA 95616, USA
[b]Armament Research, Development and Engineering Center, Picatinny, NJ 07806, USA

The influence of nanoscale reinforcement on the mechanical behavior of ultrafine-grained composites was studied. Al 5083 (Al–4.5 Mg–0.57Mn–0.25Fe) composites, with grain size of 115 nm and B$_4$C reinforcement size of 38 nm, were fabricated via cryomilling and consolidation. The result reveals that the presence of nanoparticles enhances strength by interacting with dislocations, while simultaneously retarding grain growth. Furthermore, the nanoparticles-reinforced composite exhibits enhanced plasticity relative to the same material reinforced with micrometric particles. The underlying mechanisms are discussed.
© 2011 Acta Materialia Inc. Published by Elsevier Ltd. All rights reserved.

Keywords: Nanocomposite; Ultrafine grained microstructure; Powder consolidation; Ductility; Cryomilling

Ultrafine-grained (UFG) aluminum matrix composites (grain size 100–500 nm) are of interest for weight-critical applications, given their potential to improve fuel efficiency and limit carbon dioxide emissions, particularly in light of recent reports that suggest that it may be possible to develop novel materials with ultra-high strength (>1 GPa) [1,2]. The published results suggest that the elevated strength in a UFG matrix is mostly derived from the Hall–Petch strengthening mechanism; however, it is typically achieved at the expense of tensile ductility due to the limited work hardening that is associated with the ultrafine grain sizes, which ultimately causes early strain localization. Moreover, it is indicated that the presence of micrometric ceramic particles negatively affects the resistance of the UFG matrix to sustain strain localization because the micrometric ceramic particles are prone to act as stress concentrators that promote early nucleation of cracks and voids [3]. One approach that has been successfully implemented to enhance plasticity and contain strain localization with minimal strength degradation involves the introduction of a bimodal grain size distribution (referred to as a trimodal composite) [4,5]. However, even in these composites large plastic strains were only reported for samples tested under compression, or at high strain rates

(>10^3 s^{-1}). In fact, for the samples tested in tensile tests, the elongation was found to be less than 1% [4,6,7], while monolithic UFG Al alloys can display a tensile ductility of up to 10% [8,9]. These results invite the question whether it is possible to further refine a bimodal grain architecture by reducing stress/strain localization in a trimodal composite and thereby retrieve the plasticity of the bimodal grain matrix? To that effect, spherical nanoparticles have been successfully incorporated into coarse grained (grain size >1 μm) composites to augment resistance to lattice dislocation glide via the Orowan mechanism, as well as to diminish stress localization from the particle size reduction, leading to a simultaneous increase in yield strength and ductility in coarse grained Al/Si$_3$N$_4$ (~15 nm) [10] and Al/Al$_2$O$_3$ (~90 nm) [11].

Recent studies have revealed that nanostructured metals may sustain tensile elongation if strain localization is effectively hindered. Xiang et al. [12] demonstrated that nanostructured Cu films that are bonded well on a polymer substrate can sustain tensile strains of up to 10% without any appreciable cracks and up to 30% with discontinuous microcracks. By contrast, poorly bonded Cu films form channel cracks at strains of about 2%. More recently, Fang et al. [13] showed that nanostructured Cu films confined by a coarse-grained Cu substrate can sustain a tensile true strain exceeding 100% without cracking through suppressing strain localization with a gradient grain size transition.

* Corresponding author. Tel.: +1 530 752 9568; e-mail: zhizhang@ucdavis.edu

Report Documentation Page		*Form Approved* *OMB No. 0704-0188*

1. REPORT DATE **01 JUL 2011**	2. REPORT TYPE	3. DATES COVERED **00-00-2011 to 00-00-2011**
4. TITLE AND SUBTITLE **Mechanical Behavior Of Ultrafine-grained Al Composites Reinforced With B4C Nanoparticles**		5a. CONTRACT NUMBER
		5b. GRANT NUMBER
		5c. PROGRAM ELEMENT NUMBER
6. AUTHOR(S)		5d. PROJECT NUMBER
		5e. TASK NUMBER
		5f. WORK UNIT NUMBER
7. PERFORMING ORGANIZATION NAME(S) AND ADDRESS(ES) **University of California,Department of Chemical Engineering and Materials Science,Davis,CA,95616**		8. PERFORMING ORGANIZATION REPORT NUMBER
9. SPONSORING/MONITORING AGENCY NAME(S) AND ADDRESS(ES)		10. SPONSOR/MONITOR'S ACRONYM(S)
		11. SPONSOR/MONITOR'S REPORT NUMBER(S)

12. DISTRIBUTION/AVAILABILITY STATEMENT
Approved for public release; distribution unlimited

13. SUPPLEMENTARY NOTES
Scripta Materialia 65, 1 July 2011 652-655,Government or Federal Purpose Rights License

14. ABSTRACT
The influence of nanoscale reinforcement on the mechanical behavior of ultrafine-grained composites was studied. Al 5083 (Al?4.5 Mg?0.57Mn?0.25Fe) composites, with grain size of 115 nm and B4C reinforcement size of 38 nm, were fabricated via cryomilling and consolidation. The result reveals that the presence of nanoparticles enhances strength by interacting with dislocations, while simultaneously retarding grain growth. Furthermore, the nanoparticles-reinforced composite exhibits enhanced plasticity relative to the same material reinforced with micrometric particles. The underlying mechanisms are discussed.

15. SUBJECT TERMS

16. SECURITY CLASSIFICATION OF:			17. LIMITATION OF ABSTRACT	18. NUMBER OF PAGES	19a. NAME OF RESPONSIBLE PERSON
a. REPORT **unclassified**	b. ABSTRACT **unclassified**	c. THIS PAGE **unclassified**	**Same as Report (SAR)**	**5**	

Standard Form 298 (Rev. 8-98)
Prescribed by ANSI Std Z39-18

In view of the above studies, the present work was undertaken to provide insight into the viability to retrieve plasticity by increasing resistance to dislocation glide and limiting stress/strain localization in a UFG matrix, thereby decreasing the size of the reinforcement phase to the nanometer scale and changing its morphology. B_4C particles were selected because this material is the third hardest ceramic, ranked just after diamond and cubic BN, and possesses a low density of 2.51 g cm^{-3} (20–40% lighter than SiC, Al_2O_3, Si_3N_4, AlN, cubic BN or diamond). These unique characteristics, along with other attractive properties such as high impact and wear resistance, and a high capacity for neutron absorption, renders it a good reinforcement candidate material [14,15]. In this study, UFG Al 5083 matrix composites reinforced with B_4C nanoparticles were fabricated through a powder metallurgy process. We first demonstrate that the high-strength UFG composite can undergo large plastic strain under compression and then the tensile deformation behavior is investigated.

Gas-atomized Al 5083 (Al–4.5 Mg–0.57Mn–0.25Fe, in wt.%) powder with a particle size of <45 μm (<325 mesh) was V-blended with 5 vol.% B_4C nanoparticles. The B_4C nanoparticles (designated n-B_4C hereafter) were fabricated and supplied by ARDEC (Armament Research, Development and Engineering Center, Picatinny, NJ), and had an average three-dimensional particle size of ∼38 nm (or an average cross-sectional particle size of 31 nm with a standard deviation of 11 nm), as shown in Figure 1. The powder blend was cryomilled in liquid nitrogen for 12 h. Cryomilling was conducted in a modified Svegvari attritor at a speed of 180 rpm with a ball-to-powder ratio of 32:1. After cryomilling, the average grain size of the composite powder was determined to be 30 nm by X-ray diffraction line profile analysis. The cryomilled, nanostructured Al5083/5 vol.% n-B_4C composite powder was hot vacuum degassed at 400 °C for ∼16 h (designated as sample 5-$n$$B_4C$ hereafter). For the trimodal composite samples (with coarse grain addition), 30 vol.% unmilled Al 5083 powder (with a grain size on the order of 1 μm) was V-blended with the cryomilled composite powder prior to degassing, to give a final composition of 3.5 vol.% n-B_4C, 66.5 vol.% UFG grains and 30 vol.% coarse grains (designated as sample 3.5-$n$$B_4C$–30CG hereafter). The degassed powder was then consolidated by hot isostatic pressing (HIP) at 400 °C, followed by extrusion at the same temperature with an extrusion ratio of 10:1. The microstructures of the samples were characterized using a Phillips CM-12 operating at 100 kV for grain size statistical analysis. High-angle angular dark-field imaging was conducted to examine
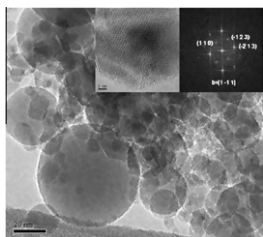
the B_4C nanoparticle dispersion using a JEOL JEM-2500SE microscope operating at 200 kV. The transmission electron microscopy (TEM) specimens were mechanically thinned to a thickness of 20 μm and then perforated using a Gatan PIPS 691 ion-milling machine. Cross-sections of the composites and fracture surfaces of tensile tested samples were examined using scanning electron microscopy (SEM). The tensile tests were carried out along the extrusion direction with an Instron 8801 universal testing machine using dog-bone-shaped specimens with a gauge length of 12 mm and a diameter of 3 mm. The compression tests were conducted using cylindrical specimens 8 mm in height and 5 mm in diameter. All the mechanical testing was performed at a strain rate of 10^{-3} s^{-1} and the strain was measured using a video extensometer with a resolution of 5 μm.

A SEM micrograph of the cross-section of the 5-$n$$B_4C$ sample in the extrusion direction is shown in Figure 2(a). The image clearly indicates that the B_4C nanoparticles (dark particles, centered around 31 nm) are homogeneously dispersed in the Al 5083 matrix. The light particles are determined to be Al_6(Mn, Fe) that exists as a non-heat-treatable intermetallic phase in the Al 5083 alloy [16]. There are occasional voids left over from consolidation (marked with a circle in Fig. 2(a)). Such residual microscale voids, although seen only rarely in our studies, may promote the initiation of shear localization and the onset of fracture, as is further addressed below. It can also be seen that a small fraction of B_4C particles in the range of 100–200 nm is present. A high-angle angular dark-field image, revealing the finer B_4C particles as well as matrix grains, is displayed in Figure 2(b). Agglomeration of reinforcing nanoparticles on grain boundaries, which was reported in micrometric-grained Al composites exceeding 4 vol.% nanoparticles [11], was not observed in our studies. Moreover, we did not observe regions denuded of reinforcing particles [7,17], which have been reported to evolve as a consequence of matrix diffusion into interparticle regions during consolidation of nanocomposite powders. Figure 2(c) is a bright-field TEM image of the Al 5083 matrix (along the extrusion direction), with the inset showing the histogram of the grain size distribution for 375 grains. The grains are mostly equiaxed, with an average size of 115 nm. The geometric mean grain

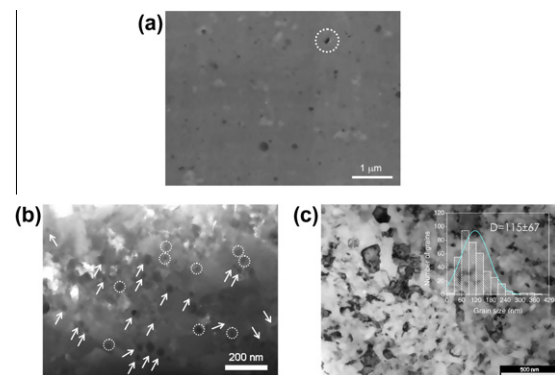**Figure 1.** TEM bright-field images of B_4C nanoparticles.

Figure 2. Microstructure of Al5083/5 vol.% n-B_4C composite: (a) SEM cross-section; (b) high-angle angular dark-field image; (c) TEM bright-field image. The n-B_4C particles at grain boundaries and within grains in (b) are marked with circles and arrows, respectively.

size of the monolithic cryomilled 5083 Al alloy consolidated through HIP followed by hot extrusion at a similar extrusion ratio is 257 nm (308/215 nm in the extrusion and transverse directions, respectively). The refined grain size in the sample is attributed to the influence of nanoparticle pinning on grain boundaries, which effectively limits grain growth [11]. For the 3.5-nB$_4$C–30CG sample, the average grain size of the CG constituent was determined to be 800 nm [6].

Figure 3(a) shows the compressive true stress–strain curves of samples 5-nB$_4$C and 3.5-nB$_4$C–30CG. The compressive true stress–strain curves of coarse-grained Al5083 alloys are also shown in Figure 3(a) for comparison. The yield strength of the 5-nB$_4$C sample (755 MPa) is 2–3 times that of conventional Al 5083 alloy strengthened by work hardening. The strength level is also much higher than that found in a monolithic Al 5083 alloy processed under similar conditions (453 MPa, where $d = 257$ nm [18]). Sample 5-nB$_4$C showed strain softening immediately after yielding (strain hardening is limited to <0.5% plastic strain). The strain softening is consistent with the characteristic microstructure, which is attributed to limited lattice dislocation accumulation in UFG Al [9]. By contrast, sample 3.5-nB$_4$C–30CG shows a moderate work hardening rate after yielding.

The strengthening mechanisms that are operative in the UFG metal matrix can be principally attributed to two factors: (i) Hall–Petch strengthening ($\Delta\sigma_{H-P}$) as a result of grain size refinement; and (ii) dislocation strengthening in the matrix ($\Delta\sigma_{dis}$), which is derived from the nucleation of additional dislocations or resistance to dislocation glide in the matrix due to the introduction of the reinforcement particles. These two factors act simultaneously, hence it is possible to estimate the yield strength of the matrix by assuming a linear superimposition of both mechanisms [19]: $\sigma_{ym} = \sigma_0 + \Delta\sigma_{H-P} + \Delta\sigma_{dis}$, where $\sigma_0 = 130$ MPa is the yield strength of coarse grained 5083 Al. The increase in yield strength contributed from dislocation strengthening is expressed via a quadratic relationship [20]:

$$\Delta\sigma_{dis} = \sqrt{\left(\Delta\sigma_{OR}^{I}\right)^2 + \left(\Delta\sigma_{OR}^{II}\right)^2 + \left(\Delta\sigma_{GND}^{EM}\right)^2 + \left(\Delta\sigma_{GND}^{CTE}\right)^2}$$

where σ_{OR}^{I} is the contribution of the Orowan strengthening from the presence of n-B$_4$C particles. With an average cross-sectional particle diameter 31 nm and particle volume fraction 0.05, $\Delta\sigma_{OR}^{I}$ is calculated to be 180 MPa using the Orowan–Ashby equation in Ref. [21]. The second Orowan strengthening term $\Delta\sigma_{OR}^{II}$ takes into account the effect from cryomilling-induced dispersoids such as oxides and nitrides and it is evaluated to be 123 MPa [21]. $\Delta\sigma_{GND}^{EM}$ accounts for the stress contribu-
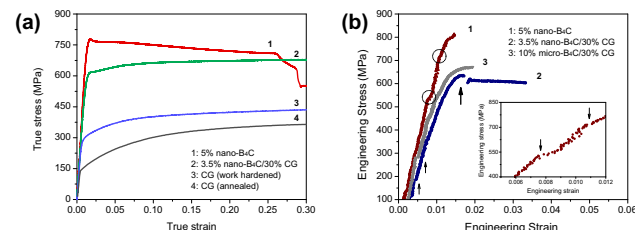
tion due to strain gradient effect associated with geometrically necessary dislocations caused by elastic modulus mismatch and it can be calculated to be 81 MPa [22]. $\Delta\sigma_{GND}^{CTE}$ is the stress contribution due to geometry necessary dislocations caused by the thermal expansion mismatch between the matrix and reinforcement. For nanoparticles (<100 nm) [23], the critical misfit strain for dislocation nucleation usually cannot be reached through the thermal expansion mismatch, hence the contribution of $\Delta\sigma_{GND}^{CTE}$ is neglected here. The yield strength increase from dislocation strengthening is then calculated to be $\Delta\sigma_{dis} = 232$ MPa. The Hall–Petch strengthening is calculated with the relation $\Delta\sigma_{H-P} = k_y/\sqrt{d}$ where k_y is a material constant and d is the mean grain size. Using $k_y = 0.15$ MPa m$^{1/2}$ for the Al–5 Mg alloy [24], $\Delta\sigma_{H-P} = 405$ MPa. The load-bearing effect from the reinforcement ($\Delta\sigma_{L-T}$) is evaluated using the modified shear lag model [25]:

$$\Delta\sigma_{L-T} = 0.5\sigma_{ym}f \cdot s = 19 \text{ MPa}$$

where s is the aspect ratio of reinforcing particles and taken to be 1. Thus the yield strength of the 5-nB$_4$C composite is estimated to be $\sigma_{yc} = \sigma_{ym} + \sigma_{L-T} = 797$ MPa. The slight overestimation relative to the experimental value (755 MPa) is likely attributed to the presence of a small number of B$_4$C particles that are larger than 100 nm such that the Orowan strengthening effect becomes invalid.

The tensile engineering stress–strain curves of samples 5-nB$_4$C and 3.5-nB$_4$C–30CG are shown in Figure 3(b). To demonstrate the effect of nanometric reinforcement, the tensile stress–strain curve of a micrometric B$_4$C-reinforced Al 5083 composite (10 vol.% B$_4$C–60 vol.% UFG–30 vol.% CG) [26] that was processed under the same thermomechanical conditions as sample 3.5-nB$_4$C–30CG is also plotted in Figure 3(b). Sample 5-nB$_4$C exhibited a plastic strain at failure of 0.3%, with pop-ins being observed prior to the catastrophic failure.

Figure 4(a) is a close-up view of sample 5-nB$_4$C after tensile testing. The inset is an enlarged view near the crack nucleation site, as marked by a white square, showing shear localization/bands that incline inward toward the sample center. The shear offset on the sample surface is obvious; signs of local melting are noticeable in the shear zone. This is consistent with the fracture surface morphology viewed from the tensile direction.

Figure 3. (a) Compressive true stress–strain curves and (b) tensile engineering stress–strain curves of UFG Al 5083/n-B$_4$C composites.
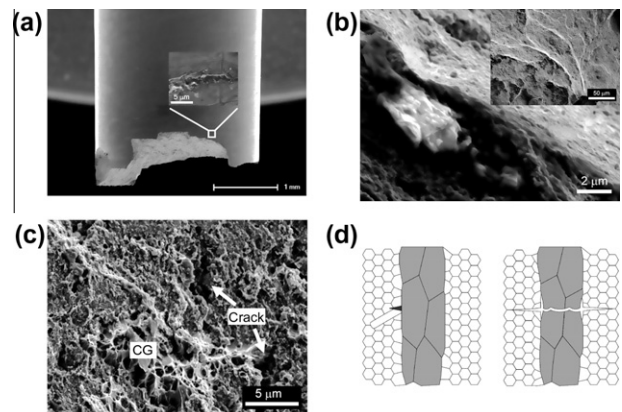

Figure 4. Fracture surface of (a and b) sample 5-nB$_4$C and (c) sample 3.5-nB$_4$C–30CG. (d) Schematic of crack initiation and propagation.

A series of shear ledges left over on the fracture surface are observed, as shown in the inset in Figure 4(b). Figure 4(b) displays an enlarged view of the shear ledge, clearly showing a bead-like signature. Signs of necking are barely visible. However, careful measurement of the sample in Figure 4(a) reveals that the diameter decreased from 2.642 to 2.581 mm from the far end to near the fracture plane; accordingly, the sample underwent a true failure strain of 4.7%. Shear lips close to 45° to the tensile direction that are ubiquitous to ductile fracture are visible. For sample 3.5-nB$_4$C–30CG in Figure 3(b), pop-ins developed at much lower stress, as indicated by thin arrows. This appears to be caused by the coarse grains, which yield first, noting that the pop-in stress is between the yield stress of annealed and work hardened CG Al 5083 alloy. A strain jump associated with microcrack development, as shown by a thick arrow, is recorded during plastic deformation after global yielding. It is worth noting that the nucleation of the microcrack does not lead to immediate catastrophic failure and the sample was able to survive the tensile instability until failure at a strain of 3%, suggesting that crack propagation is indeed delayed by the coarse grains.

Evidence of the influence of the coarse grains on crack propagation is shown by the fracture surface in Figure 4(c). By contrast, it took 10 vol.% micrometric B$_4$C to reach a similar yield stress, but the composite failed early at a strain of 1% and a strain jump associated with microcrack arresting was not observed.

On the basis of microstructural and mechanical characteristics observed in the present study, the toughening mechanism in the sample 3.5-nB$_4$C–30CG is illustrated in Figure 4(d). Shear bands are nucleated first in the nanostructured regions and develop into microcracks; the microcracks then propagate until they reach the coarse grain regions, the coarse grains impede further crack propagation by blunting the crack or by delamination of the interfaces between the coarse- and fine-grained regions. As tensile strain accumulates during deformation, cavitation and necking within the coarse-grained bands will develop. In the final stage, dimples will evolve in the coarse-grained regions, ultimately leading to fracture. The delamination at the interfaces and the necking deformation in ductile coarse-grained regions will cause significant energy loss, resulting in enhanced tensile ductility. Shear banding has been widely reported in UFG body-centered cubic alloys [27,28]. In UFG fcc alloys, shear banding is documented in UFG Al–Mg [29] and nanostructured Cu [30]. It is worth noting that these materials are all consolidated from powders; it is possible that shear localization is more easily triggered in such materials due to the presence of residual porosity and/or prior particle boundaries. It is thus anticipated that complete elimination of processing artifacts, such as prior particle boundaries, will further enhance ductility.

In summary, the present results suggest that it is possible to limit stress/strain localization and thereby retrieve plasticity by decreasing the size of the reinforcement phase to the nanometer scale. Our results show that nanoparticles enhance strength by interacting with dislocations, while simultaneously retarding grain growth. Finally, the nanoparticles-reinforced composite exhibits enhanced plasticity relative to the same material reinforced with micrometric particles.

[1] S.C. Tjong, Adv. Eng. Mater. 9 (2007) 639–652.
[2] W. Xu, X. Wu, T. Honma, S.P. Ringer, K. Xia, Acta Mater. 57 (2009) 4321–4330.
[3] R. Vogt, Z. Zhang, E. Huskins, B. Ahn, S. Nutt, K.T. Ramesh, E.J. Lavernia, J.M. Schoenung, Mater. Sci. Eng. A 527 (2010) 5990–5996.
[4] R.G. Vogt, Z. Zhang, T.D. Topping, E.J. Lavernia, J.M. Schoenung, J. Mater. Proc. Technol. 209 (2009) 5046–5053.
[5] H. Zhang, J. Ye, S.P. Joshi, J.M. Schoenung, E.S.C. Chin, K.T. Ramesh, Scripta Mater. 59 (2008) 1139–1142.
[6] J. Ye, B.Q. Han, Z. Lee, B. Ahn, S.R. Nutt, J.M. Schoenung, Scripta Mater. 53 (2005) 481–486.
[7] F. Tang, M. Hagiwara, J.M. Schoenung, Mater. Sci. Eng. A 407 (2005) 306–314.
[8] N. Tsuji, Y. Ito, Y. Saito, Y. Minamino, Scripta Mater. 47 (2002) 893–899.
[9] C.Y. Yu, P.W. Kao, C.P. Chang, Acta Mater. 53 (2005) 4019–4028.
[10] Z.Y. Ma, Y.L. Li, Y. Liang, F. Zheng, J. Bi, S.C. Tjong, Mater. Sci. Eng. A 219 (1996) 229–231.
[11] Y.C. Kang, S.L.I. Chan, Mater. Chem. Phys. 85 (2004) 438–443.
[12] Y. Xiang, T. Li, Z.G. Suo, J.J. Vlassak, Appl. Phys. Lett. 87 (2005).
[13] T.H. Fang, W.L. Li, N.R. Tao, K. Lu, Science. 331 (2011) 1587–1590.
[14] I. Topcu, H.O. Gulsoy, N. Kadioglu, A.N. Gulluoglu, J. Alloys Compd. 482 (2009) 516–521.
[15] M. Khakbiz, F. Akhlaghi, J. Alloys Compd. 479 (2009) 334–341.
[16] Y.S. Sato, S.H.C. Park, H. Kokawa, Metall. Mater. Trans. A 32 (2001) 3033–3042.
[17] S. Kamrani, R. Riedel, S.M.S. Reihani, H.J. Kleebe, J. Composite Mater. 44 (2010) 313–326.
[18] D.B. Witkin, E.J. Lavernia, Prog. Mater. Sci. 51 (2006) 1–60.
[19] S.P. Joshi, C. Eberl, B. Cao, K.T. Ramesh, K.J. Hemker, Exp. Mech. 49 (2009) 207–218.
[20] S. Scudino, G. Liu, M. Sakaliyska, K.B. Surreddi, J. Eckert, Acta Mater. 57 (2009) 4529–4538.
[21] B.Q. Han, Z. Lee, S.R. Nutt, E.J. Lavernia, F.A. Mohamed, Metall. Mater. Trans. A 34 (2003) 603–613.
[22] F. Tang, I.E. Anderson, T. Gnaupel-Herold, H. Prask, Mater. Sci. Eng. A 383 (2004) 362–373.
[23] M. Taya, K.E. Lulay, D.J. Lloyd, Acta Metall. Mater. 39 (1991) 73–87.
[24] D.J. Lloyd, S.A. Court, Mater. Sci. Technol. 19 (2003) 1349–1354.
[25] V.C. Nardone, K.M. Prewo, Scripta Metall. 20 (1986) 43–48.
[26] R. Vogt, Ph.D. Thesis, University of California, Davis, 2010.
[27] J.E. Carsley, A. Fisher, W.W. Milligan, E.C. Aifantis, Metall. Mater. Trans. A 29 (1998) 2261–2271.
[28] Q. Wei, D. Jia, K.T. Ramesh, E. Ma, Appl. Phys. Lett. 81 (2002) 1240–1242.
[29] G.J. Fan, H. Choo, P.K. Liaw, E.J. Lavernia, Acta Mater. 54 (2006) 1759–1766.
[30] S. Cheng, E. Ma, Y.M. Wang, L.J. Kecskes, K.M. Youssef, C.C. Koch, U.P. Trociewitz, K. Han, Acta Mater. 53 (2005) 1521–1533.